Processing and Application of Ceramics 19 [1] (2025) 50–56
https://doi.org/10.2298/PAC2501050W

Fabrication, structure and complex dielectric properties of $SrFeO_3$-$LaFeO_3$ ceramic composites

Xiaoyu Wu, Wei Li, Ziheng Huang, Depeng Wang, Weitian Wang*

School of Physics and Electronic Information, Yantai University, Yantai 264005, P.R. China

Received 26 November 2024; Received in revised form 10 February 2025; Accepted 1 March 2025

Abstract

In this study, $SrFeO_3$-$LaFeO_3$ ceramic composite was prepared from mixture of $SrFeO_3$ and $LaFeO_3$ powders (synthesized by solid state reaction method) by pressing and sintering at 1400 °C for 6 h. The composite exhibits single orthorhombic structure with coexistence of $SrFeO_3$ and $LaFeO_3$ phases. Chemical composition and complex dielectric properties were investigated. The obtained permittivity of the $SrFeO_3$-$LaFeO_3$ composite is 2 to 3 times higher than that of the pure $SrFeO_3$ or $LaFeO_3$ perovskite samples. The observed dielectric behaviour can be explained by the localized dipolar effect and dielectric relaxation processes, arising from the presence of mixed-valence state of Fe (i.e., Fe^{2+}/Fe^{3+}/Fe^{4+} pairs) and oxygen vacancies with activation energies of 0.38 and 0.73 eV, respectively. Resistances of grain boundaries and grains were revealed by impedance spectroscopy.

Keywords: *$SrFeO_3$-$LaFeO_3$ ceramics, structure, dielectric properties, impedance analysis*

I. Introduction

Perovskite oxides (ABO_3) have gained significant attention due to their versatile electronic and dielectric properties, which make them suitable for a wide range of applications, from solid-state devices to sensors. One of the more appealing features of these materials lies in the fact that they can be easily modified by doping with other elements, which allows for the tuning of their properties for specific applications.

In the family of ABO_3, $SrFeO_3$ (SFO) and $LaFeO_3$ (LFO) stand out as important ferrites due to their thermal stability, dielectric, ferroelectric and ferromagnetic properties. It has been reported that SFO exhibits ferromagnetic behaviour at room temperature, while LFO is an antiferromagnetic material with the Néel temperature around 750 K. Many research achievements on SFO and LFO have been reported in various state-of-the-art fields such as solid oxide fuel cells, photocatalysis, chemical sensors, magnetic material advancements and the innovation of electrode materials [1–7]. Huang *et al.* [8] have reported that the creation of oxygen vacancies in $La_{1-x}Sr_xFeO_3$ nanoparticles is crucial for the charge compensation during the substitution of high-valence cation ions with low-valence ones, which in turn affects the dielectric properties. Similarly, Cao *et al.* [9] discovered that $La_{1-x}Na_xFeO_3$ crystals exhibit a dielectric constant as high as 10^5 at low frequencies. Additionally, it has been proved by Omari *et al.* [10] that the solid solution of $0.97(PbTiO_3)$-$0.03(LaFeO_3)$ showed an optical bandgap of 2.032 eV, indicating it as a potential material for solar cell technologies. Up to now, cation ions with different valence states, such as monovalent (Na [9], K [11], Ag [12]), divalent (Pb [3], Sr [14], Zn [14]), trivalent elements (Co [15], Cr [16], Al [17]) and tetravalent elements (Ti [18]) have been reported as dopants entering into $LaFeO_3$ crystal lattice, and their effects on magnetic or electrical and optical properties have been investigated.

The composites formed by combining SFO and LFO can potentially yield unique properties that are not present in either of the individual components. This article aims to explore the dielectric properties of $0.5SrFeO_3$-$0.5LaFeO_3$ (SFO-LFO) composites, providing insights into how these properties can be tailored for specific applications. Our results show that the SFO-LFO composites exhibit excellent dielectric properties which can be explained by the dipolar effect, originating from the mixed-valence state of Fe^{2+}/Fe^{3+}/Fe^{4+} pairs and oxygen vacancies.

* Corresponding authors: tel: +86 13573512787,
e-mail: *wtwang@ytu.edu.cn*

II. Experimental

The SFO and LFO powders were prepared by using the solid-state reaction method. Firstly, the SFO powder was synthesized by employing high-purity chemical reagents $SrCO_3$ (≥99.9%, Macklin Chemical Co. Ltd, Shanghai, China) and Fe_2O_3 (≥99.9%, Macklin Chemical Co. Ltd, Shanghai, China). The raw chemical materials were meticulously weighed according to the stoichiometric ratio and thoroughly mixed. The mixed precursors were finely ground and subjected to a solid-state calcination process at 1250 °C in a muffle furnace for 8 h to obtain the SFO powders. Secondly, the LFO powder was synthesized by using the stoichiometric La_2O_3 and Fe_2O_3 raw materials and the same process for producing the SFO powder was carried out. Finally, the SFO and LFO powders were mixed with equal mole ratio to obtain the SFO-LFO precursor. After being ground in an agate pestle and mortar for a period of 1 h, the composite powders were pressed (14 MPa) into cylindrical pellets of uniform thickness using a pellet press. The pellets were sintered at 1400 °C for 6 h to form ceramic samples.

The bulk densities of the samples were measured by the Archimedes method. The crystal structure of the prepared samples was investigated using X-ray diffraction (XRD) with Cu Kα radiation (λ = 1.5418 Å) over a 2θ range of 20°–80°, employing an X'Pert3 Powder diffractometer (PANalytical, The Netherlands). Structural analysis of the XRD data was performed using the General Structure Analysis System (GSAS) and VESTA (JP-Mineral.org, Ibaraki, Japan) software. Surface micromorphology was observed by scanning electron microscopy (SEM) using a JEOL-JSM-7610F operated at 2 kV acceleration voltages. X-ray photoelectron spectroscopy (XPS) was used to analyse the composition and valence state of the specimens utilizing a monochromatic Al Kα X-ray source from the ESCALAB 250Xi, a device manufactured by Thermo Electron Corporation in the USA. The dielectric properties were investigated using a HIOKI 3532-50 LCR HiTester and an HP4194A analyser, which allowed for measurements across a frequency range of 100 Hz to 1 MHz. The measurements were conducted on the samples with silver electrodes uniformly applied to both sides of the pellets.

III. Results and discussion

The Rietveld refinement was performed by using the GSAS program to analyse the XRD patterns of the sintered samples and corresponding results are shown in Fig. 1. As shown in Figs. 1a and 1b, all the diffraction patterns demonstrate excellent crystalline quality and the presence of iron-based perovskite phases. The diffraction peaks in Fig. 1a can be confirmed and indexed with the standard reference pattern of LFO in orthorhombic structure (PDF #37-1493), while that in Fig. 1b can be confirmed with the pattern of SFO (PDF #40-0906). No impurities or alternative phases can be detected. The determined lattice parameters are: a = 5.566 Å, b = 7.854 Å and c = 5.553 Å for the LFO, and a = 10.97 Å, b = 7.702 Å and c = 5.471 Å for the SFO samples. Figure 1c shows results of the Rietveld refinement analysis of the SFO-LFO composite. As it is known, the ionic radius of Sr^{2+} is 118 pm, and that of La^{3+} ions is 102 pm. The results revealed the coexistence of two phases of SFO (*Pnna*) and LFO (*Pbnm*) for the composites, indicating that the crystalline structures of SFO and LFO coexist for the SFO-LFO composite. The obtained mass fraction of SFO is about 44.1%, while that of LFO is about 55.9% (Fig. 1c). The calculated molar ratio of SFO and LFO is approximately 1:1, which corresponds well with the molar ratio in the prepared 0.5SFO-0.5LFO composite.

Densification of the prepared ceramics was analysed by density measurement which were 83, 85 and 94 %TD for the SFO, LFO and SFO-LFO samples, respectively.

SEM images of the prepare samples are presented

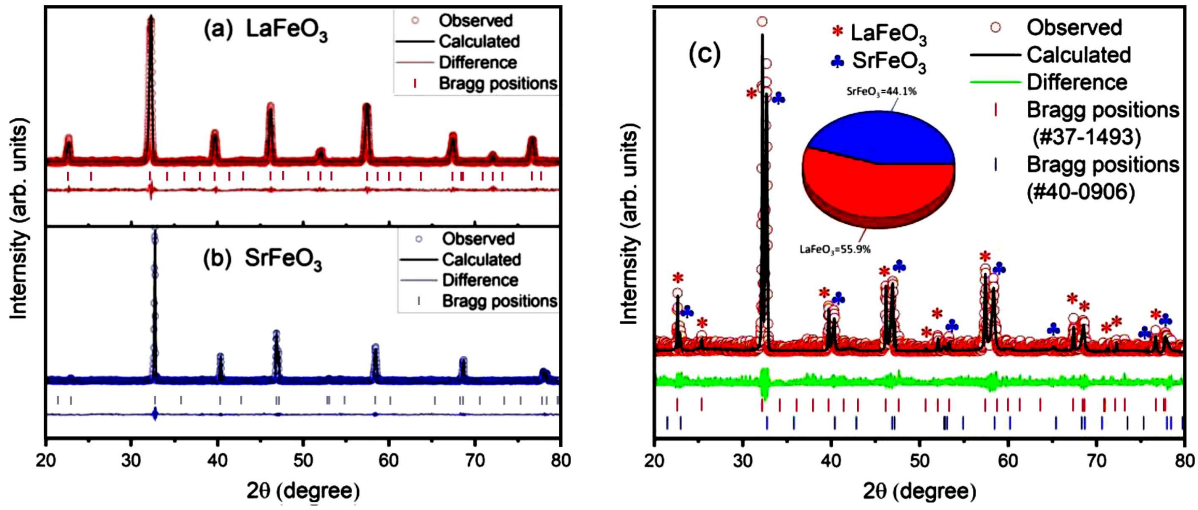

Figure 1. XRD Rietveld refinement results of: a) LFO, b) SFO and c) SFO-LFO sintered samples (the inserted pie chart shows the mass fraction of LFO and SFO)

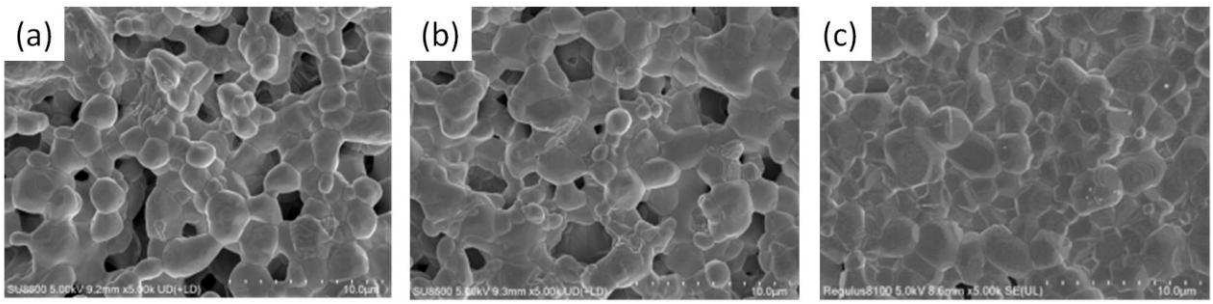

Figure 2. SEM images of: a) SFO, b) LFO and SFO-LFO sintered samples

in Fig. 2. The morphology of the SFO (Fig. 2a) and LFO ceramics (Fig. 2b) shows the existence of grains (3–5 μm) and intergranular porosity. The pores are interconnected with one another, forming a porous microstructure. A dense structure for the SFO-LFO composite is shown in Fig. 2c. The equimolar blending of SFO and LFO appears to be effective in mitigating porosity. By using Archimedes' method, it was quantitatively determined that the porosity was reduced by approximately 10%. Similar results were reported for $CaTiO_3$-$FeTiO_3$ and $CaTiO_3$-$BiFeO_3$ composites [19,20]. These characteristics may have a direct impact on the dielectric properties of the prepared SFO-LFO composite.

Figure 3 displays XPS spectra for the fabricated SFO-LFO composite. The survey XPS spectrum (Fig. 3a) suggests the presence of La, Sr, Fe, O and C. The binding energy of C 1*s* at 284.8 eV was used to calibrate the data. The Sr 3*d* high-resolution XPS spectrum (Fig. 3b) shows characteristic peaks located at 133.6 and 135.4 eV, respectively, suggesting that the Sr ions are in Sr^{2+} states. The scan of the La 2*p* spectra (Fig. 3c) exhibit peaks for La $2p_{5/2}$ and La $2p_{3/2}$ at 883.7 and 850.7 eV, respectively, with characteristic satellite peaks in accordance with the standard La^{3+} [21]. The Fe 2*p* spectrum (Fig. 3d) displays a doublet assigned to $2p_{3/2}$ and $2p_{1/2}$, respectively. The $2p_{3/2}$ peak is resolved into three peaks at 709.7, 710.7 and 713 eV, attributed to Fe^{2+}, Fe^{3+} and Fe^{4+}, respectively. This is in agreement with the reports by Mullet *et al.* [22], indicating a mixed-valence state of iron in the samples. The O 1*s* XPS spectra (Fig. 3e) is deconvoluted into three Gaussian peaks at 529.8, 530.7 and 531.8 eV, which can be ascribed to lattice oxygen, oxygen vacancies and surface-adsorbed oxygen, respectively. These findings are in line with the results reported by Wang *et al.* [23] on $BaFeO_{3-\delta}$ ceramics.

The frequency dependence of the real part of the dielectric constant (ε') and tangent loss ($\tan\delta$) are illustrated in Fig. 4. As shown in Figs. 4a and 4b, the dielectric constant at lower frequencies is large due to the dipolar polarization in the SFO and LFO ceramics. As frequency increases, the dielectric constant is reduced because electron movement may not synchronize with

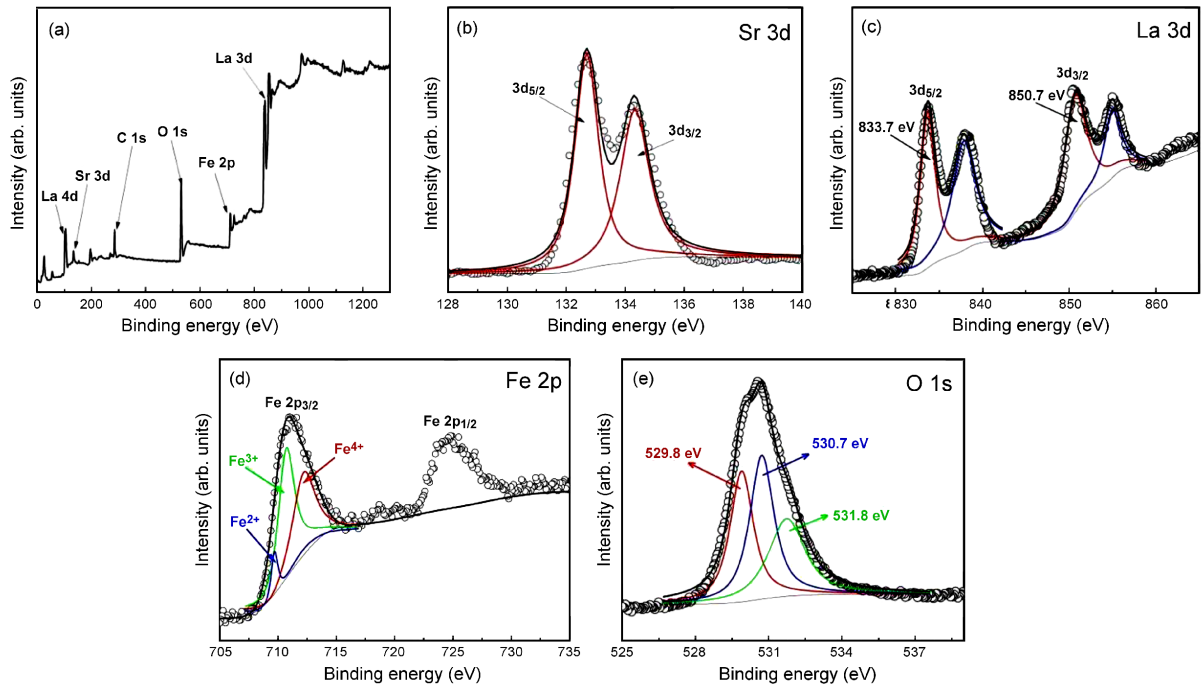

Figure 3. Typical XPS spectra of SFO-LFO composite: a) survey investigation, b) Sr 3*d*, c) La 3*d*, d) Fe 3*d* and e) O 1*s*

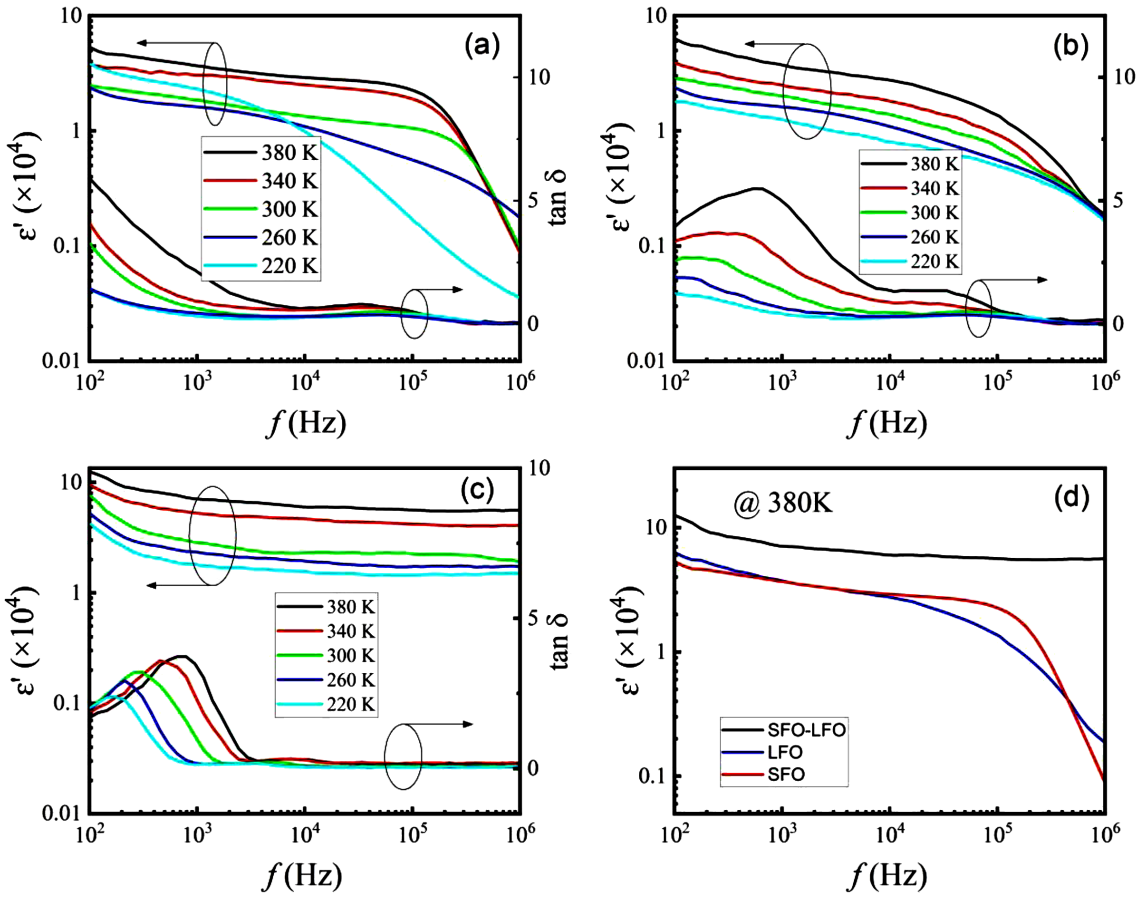

Figure 4. Frequency dependence of ε' and tanδ for: a) SFO, b) LFO and c) SFO-LFO ceramics at different temperatures, and d) comparison of ε' values for SFO, LFO and SFO-LFO samples at 380 K

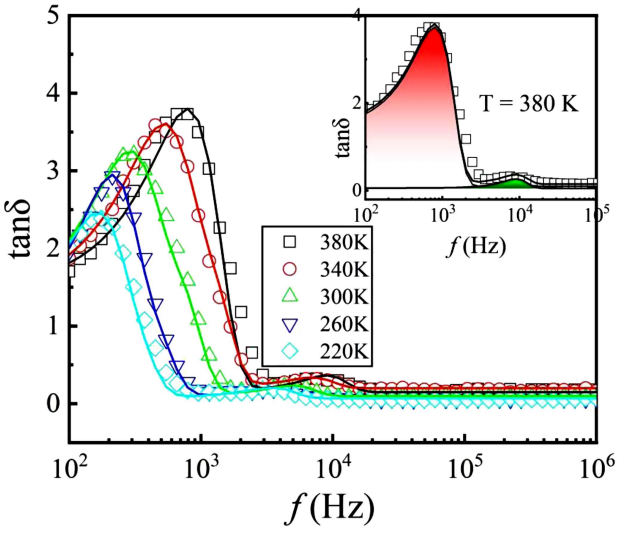

Figure 5. Variation of tanδ with frequency at different temperatures for SFO-LFO composite (solid curves are the least-squares fitting data by the Gaussian function and inset shows the typical result at T = 380 K)

the fluctuations of the external electric field [24,25]. As for the SFO-LFO composites (Fig. 4c), the obtained values of ε' not only exceed those of SFO and LFO, but exhibit good frequency stability. This enhancement may originate from the dipolar effect arising from the $Fe^{4+}/Fe^{3+}/Fe^{2+}$ ion pairs, as shown in the XPS analysis (Fig. 3d), within the perovskite framework of iron. The hopping of electrons between these ions induces dipolar polarization which aligns the dipoles in response to a varying electric field, resulting in the increased dielectric properties. Comparison of ε' values of the SFO, LFO and SFO-LFO samples at 380 K is shown in Fig. 4d. At low frequencies, the ε' value of the SFO-LFO composite is about twice as high as that of the SFO or LFO ceramics. The enhancement is more pronounced in the high-frequency region. Similar results have been reported in other transition metal oxides [26].

The variation of tan δ in Fig. 4 shows peaks at different frequencies, indicating the presence of a relaxation process. Typical analysis of the tan δ data for the SFO-LFO composite is shown in Fig. 5. After fitting the data, the variations of tan δ can be decomposed into two peaks, corresponding to the relaxations at high- and low-frequencies. Typical result for T = 380 K is shown in the inset of Fig. 5. As the temperature increases, the respective peak positions shift to higher frequencies. For a relaxation related to thermally activated process, the activation energy E_a can be calculated using the Arrhenius law:

$$f = f_0 \cdot \exp\left(-\frac{E_a}{k_B \cdot T}\right) \tag{1}$$

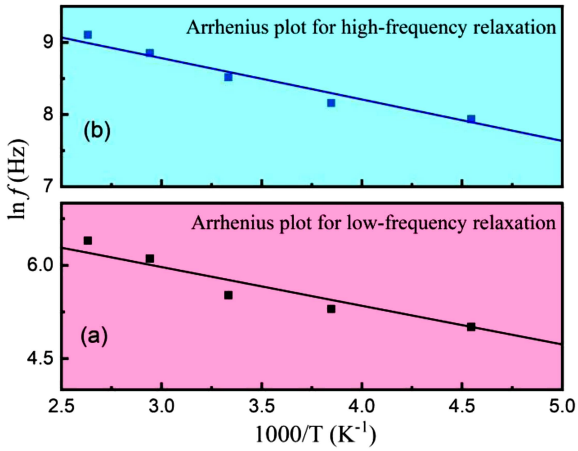

Figure 6. The Arrhenius plots for: a) the low-frequency relaxation peak and b) the high-frequency relaxation peak

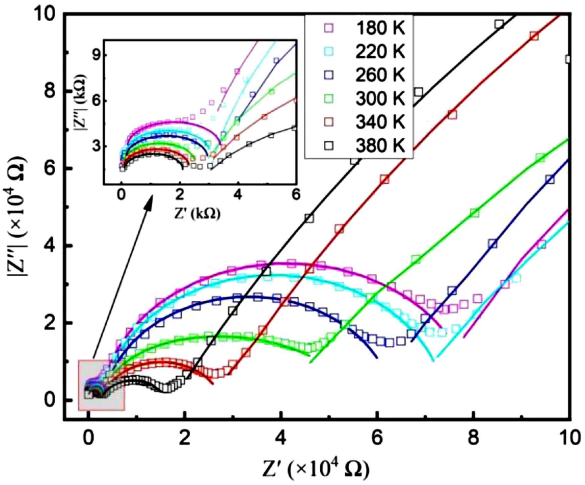

Figure 7. Complex impedance plots for the prepared SFO-LFO composite at different temperatures (solid lines are the best-fitting results)

where f_0 stands for a pre-exponential factor, k_B is the Boltzmann parameter and T represents the peak temperature.

The Arrhenius plots for the two relaxations are shown in Fig. 6. The presence of a strong linear correlation between $1/T$ and $\ln f$ gives the activation energies (E_a) for the high- and low-frequency relaxations as 0.38 and 0.73 eV, respectively. As reported by Wan *et al.* [27] and Dang *et al.* [28], 0.3–0.4 eV in the frequency range of 5×10^3–5×10^4 Hz is a typical activation energy for the polaron relaxation caused by the exchange of electrons between multivalent transition metal ions. The obtained $E_a = 0.38$ eV can be attributed to the activated hopping of small polarons between Fe^{2+}, Fe^{3+} and Fe^{4+} ions. The oxide vacancies have a major contribution to the activation energy of 0.73 eV [28].

To separate the dielectric responses from different electroactive regions in the SFO-LFO composite, complex impedance analysis was performed in the temperature range of 180–380 K. The obtained Z' vs. Z'' spectra are presented in Fig. 7. Generally, due to the different relaxation times, the impedance responses from high to low frequency can be attributed to the responses of grains, grain boundaries and electrodes, respectively [29]. As shown in Fig. 7, semicircles with large radii can be observed in the low-frequency region which can be assigned to the dielectric response from electrodes. The sequential two regions from left to right correspond, respectively, to the dielectric response from grain boundaries and bulk grains. The presence of intergranular porosity, defects and oxygen vacancies at the grain boundaries restricts the movement of charge carriers, resulting in the grain boundary impedance being significantly higher than that of grains [30,31]. With the frequency increasing, the radius of the observed semicircles increases with decreasing temperature, which suggests the dependence of the grain and grain boundary resistances on the temperature, indicating the semiconducting behaviour of the material. As the operating frequency further increases, small semicircles can be found in the high-frequency region, as shown in the inset of Fig. 7. The temperature effect on the radius of these semicircles is similar to the results of grain boundaries. The dependence of the calculated resistance of grain boundaries (R_{gb}) and the grains (R_g) on temperature is shown in Fig. 8. As it is known, when the mobility of charge carriers is temperature activated, the resistance R depends on the temperature T according to the equation [32]:

$$R = R_0 \cdot \exp\left(\frac{B}{T}\right) \tag{2}$$

where R_0 and B are material-related constants. The linear relationship of $\ln(R_{gb}) \sim 1/T$ and $\ln(R_g) \sim 1/T$ provides an evidence of negative temperature coefficient of resistance, which implies that the prepared SFO-LFO composite is a stable semiconductor material.

IV. Conclusions

$SrFeO_3$-$LaFeO_3$ (SFO-LFO) ceramic composite was prepared from mixture of $SrFeO_3$ and $LaFeO_3$ powders

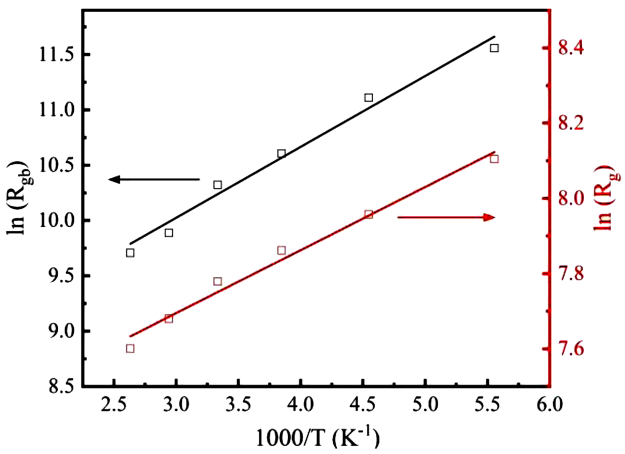

Figure 8. Plots of grain boundaries $\ln(R_{gb})$ and the grain resistance $\ln(R_g)$ against $1/T$ (solid lines are linear fits to the data)

(synthesized by solid state reaction method) by pressing and sintering at 1400 °C for 6 h. XRD results revealed the coexistence of two phases (orthorhombic SFO and LFO) in the SFO-LFO composite. In addition, it was shown that densification of the SFO-LFO composite was improved in comparison to the pure SFO or LFO ceramics.

The value of dielectric constant ε' for the SFO-LFO composite is at least twice as much as that of the pure SFO or LFO ceramics. The relaxations at high- and low-frequencies were considered to be originated from the $Fe^{2+}/Fe^{3+}/Fe^{4+}$ pairs and oxide vacancies, with activation energies of 0.38 and 0.73 eV, respectively. Impedance spectroscopy, used to determine the relationship between temperature and resistance of grain and grain boundary, indicates the semiconducting behaviour of the fabricated material. The obtained results suggest that the SFO-LFO composite exhibits excellent dielectric properties due to its unique structure and composition, which makes it a promising candidate for applications in electronic capacitors and optoelectronic devices.

Acknowledgement: This work was supported by the National Natural Science Foundation of China (No. 12374031) and the Graduate Innovation Foundation of Yantai University (No. GGIFYTU2315).

References

1. A. Maignan, C. Martin, N. Nguyen, B. Raveau, "Magnetoresistance in the ferromagnetic metallic perovskite $SrFe_{1-x}Co_xO_3$", *Solid State Sci.*, **3** [1-2] (2001) 57–63.
2. Q. Zhang, F. Saito, "Effect of Fe_2O_3 crystallite size on its mechanochemical reaction with La_2O_3 to form $LaFeO_3$", *J. Mater. Sci.*, **36** [9] (2001) 2287–2290.
3. S. Kumar, J. Pal, S. Kaur, R. Kaur, P. D. Babu, M. Singh, A. Singh, "The effect of aliovalent Pb^{2+} dopant on the magnetic and magneto dielectric properties of $LaFeO_3$ solid solutions", *J. Magn. Magn. Mater.*, **467** (2018) 89–95.
4. N. Afifah, R. Saleh, "Synthesis, characterization and catalytic properties of perovskite $LaFeO_3$ nanoparticles", *J. Phys. Conf. Ser.,* **710** (2016) 012030.
5. K. Shinde, C. Hwang, M. Manawan, Y.S. Choi, S. Park, Y. Jo, "Magnetocaloric effect and griffiths phase analysis in a nanocrystalline Ho_2NiMnO_6 and Ho_2CoMnO_6 double perovskite", *RSC Advances*, **13** (2023) 9099–9108.
6. S. Ogawa, S. Tamura, H. Yamane, T. Tanabe, M. Saito, T. Motohashi, "New triclinic perovskite-type oxide $Ba_5CaFe_4O_{12}$ for low-temperature operated chemical looping air separation", *J. Am. Chem. Soc.*, **145** [41] (2023) 22788–22795.
7. N. Labhasetwar, G. Saravanan, S.K. Megarajan, N. Manwar, R. Khobragade, P. Doggali, F. Grasset, "Perovskite-type catalytic materials for environmental applications", *Sci. Technol. Adv. Mater.*, **16** [3] (2015) 036002.
8. L. Huang, L. Cheng, S. Pan, Y. He, C. Tian, J. Yu, H. Zhou, "Effects of Sr doping on the structure, magnetic properties and microwave absorption properties of $LaFeO_3$ nanoparticles", *Ceram. Int.*, **46** [17] (2020) 27352–27361.
9. E. Cao, Y. Qin, T. Cui, L. Sun, W. Hao, Y. Zhang, "Influence of Na doping on the magnetic properties of $LaFeO_3$ powders and dielectric properties of $LaFeO_3$ ceramics prepared by citric sol-gel method", *Ceram. Int.*, **43** [10] (2017) 7922–7928.
10. L.H. Omari, H. Lemziouka, M. Haddad, T. Lamhasni, "Structural, optical and electrical properties of $0.97(PbTiO_3)$-$0.03(LaFeO_3)$ solid solutions", *Mater. Today: Proceed.*, **13** (2019) 1205–1214.
11. M.B. Bellakki, V. Manivannan, "Solution combustion synthesis of $(La,K)FeO_3$ orthoferrite ceramics: Structural and magnetic property studies", *Bull. Mater. Sci.*, **33** (2010) 611–618.
12. M.B. Bellakki, B.J. Kelly, V. Manivannan, "Synthesis, characterization, and property studies of (La, Ag) FeO_3 ($0.0 \leq x \leq 0.3$) perovskites", *J. Alloys Compd.*, **489** [1] (2010) 64–71.
13. Q. Ming, M.D. Nersesyan, A. Wagner, J. Ritchie, J.T. Richardson, D. Luss, A.J. Jacobson, Y.L. Yang, "Combustion synthesis and characterization of Sr and Ga doped $LaFeO_3$", *Solid State Ionics*, **122** [1-4] (1999) 113–121.
14. K. Mukhopadhyay, A.S. Mahapatra, P.K. Chakrabarti, "Multiferroic behavior, enhanced magnetization and exchange bias effect of Zn substituted nanocrystalline $LaFeO_3$ ($La_{(1-x)}Zn_xFeO_3$, x = 0.10, and 0.30)", *J. Magn. Magn. Mater.*, **329** (2013) 133–141.
15. I.O. Troyanchuk, D.V. Karpinsky, R. Szymczak, H. Szymczak, "Effect of oxygen deficit on magnetic properties of $LaCo_{0.5}Fe_{0.5}O_3$", *J. Magn. Magn. Mater.*, **298** [1] (2006) 19–24.
16. A.P.B. Selvadurai, V. Pazhanivelu, C. Jagadeeshwaran, R. Murugaraj, I.P. Muthuselvam, F.C. Chou, "Influence of Cr substitution on structural, magnetic and electrical conductivity spectra of $LaFeO_3$", *J. Alloys Compd.*, **646** (2015) 924–931.
17. S. Acharya, P.K. Chakrabarti, "Some interesting observations on the magnetic and electric properties of Al^{3+} doped lanthanum orthoferrite ($La_{0.5}Al_{0.5}FeO_3$)", *Solid State Commun.*, **150** [27-28] (2010) 1234–1237.
18. S. Phokha, S. Hunpratup, S. Pinitsoontorn, B. Putasaeng, S. Rujirawat, S. Maensiri, "Structure, magnetic, and dielectric properties of Ti-doped $LaFeO_3$ ceramics synthesized by polymer pyrolysis method", *Mater. Res. Bull.*, **67** (2015) 118–125.
19. N. Gouitaa, F.Z. Ahjyaje, T. Lamcharfi, F. Abdi, M. Haddad, "Colossal dielectric constant (CDC) response in $0.5CaTiO_3$-$0.5FeTiO_3$ composites", *J. Mater. Res.*, **38** [9] (2023) 2486–2494.
20. L.L. Xiang, J. Liu, J.N. Zuo, X.T. Guo, L.J. Wang, T.L. Sun, D. Xu, "Effect of co-substitution of $Na_{0.5}Bi_{0.5}TiO_3$ and $CaTiO_3$ on the structure and properties of $BiFeO_3$ ceramics", *J. Mater. Sci. Mater. Electron.*, **33** [27] (2022) 21838–21851.
21. M.M. Natile, A. Galenda, A. Glisenti, "From La_2O_3 to $LaCoO_3$: XPS analysis", *Surf. Sci. Spectra.*, **15** [1] (2008) 1–13.
22. M. Mullet, V. Khare, C. Ruby, "XPS study of Fe(II)-Fe(III)(oxy) hydroxycarbonate green rust compounds", *Surf. Interface Anal.*, **40** [3-4] (2008) 323–328.
23. R. Ahmed, S.T. Wang, J. Sun, J. Wang, T.Y. Li, Y. Yu, Q.J. Li, C.C. Wang, "Colossal dielectric behavior in $BaFeO_{3-\delta}$ ceramics", *Ceram. Int.*, **45** [10] (2019) 13484–13487.
24. N. Zarrin, S. Husain, S. Sharma, A. Somvanshi, S.

Manzoor, W. Khan, "Thermally stimulated small polaron promoted conduction mechanism in Fe-doped $La_{0.7}Sm_{0.3}CrO_3$", *J. Phys. Chem. Solids.*, **138** (2020) 109281.
25. M. Abushad, W. Khan, S. Naseem, S. Husain, M. Nadeem, A. Ansari, "Influence of Mn doping on microstructure, optical, dielectric and magnetic properties of $BiFeO_3$ nanoceramics synthesized via sol-gel method", *Ceram. Int.*, **45** [6] (2019) 7437–7445.
26. A. Sagdeo, K. Gautam, P.R. Sagdeo, M.N. Singh, S.M. Gupta, A.K. Nigam, R. Rawat, A.K. Sinha, H. Ghosh, T. Ganguli, A. Chakrabarti, "Large dielectric permittivity and possible correlation between magnetic and dielectric properties in bulk $BaFeO_{3-\delta}$", *Appl. Phys. Lett.*, **105** [4] (2014) 042906.
27. F. Wan, X. Hua, Q. Guo, "Modulation of the structural, magnetic, and dielectric properties of $YMnO_3$ by Cu doping", *Materials*. **17** [12] (2024) 2929.
28. N.T. Dang, D.P. Kozlenko, N. Tran, B.W. Lee, T.L. Phan, R.P. Madhogaria, V. Kalappattil, D.S. Yang, S.E. Kichanov, E.V. Lukin, B.N. Savenko, P. Czarnecki, T.A. Tran, V.L. Vo, L.T.P. Thao, D.T. Khan, N.Q. Tuan, S.H. Jabarov, M.H. Phan, "Structural, magnetic and electronic properties of Ti-doped $BaFeO_{3-\delta}$ exhibiting colossal dielectric permittivity", *J. Alloy. Compd.*, **808** (2019) 151760.
29. M.R. Biswal, J. Nanda, N.C. Mishra, S. Anwar, A. Mishra, "Dielectric and impedance spectroscopic studies of multiferroic $BiFe_{1-x}Ni_xO_3$", *Adv. Mater. Lett.*, **5** [9] (2014) 531–537.
30. T. Futazuka, R. Ishikawa, N. Shibata, Y. Ikuhara, "Grain boundary structural transformation induced by cosegregation of aliovalent dopants", *Nat. Commu.*, **13** [1] (2022) 5299.
31. Y. Feng, W.L. Li, Y.F. Hou, Y. Yu, W.P. Cao, T.D. Zhang, W.D. Fei, "Enhanced dielectric properties of PVDFHFP/$BaTiO_3$-nanowires composites induced by interfacial polarization and wire-shape", *J. Mater. Chem. C.*, **3** [6] (2015) 1250–1260.
32. A. Feteira, "Negative temperature coefficient resistance (NTCR) ceramic thermistors: An industrial perspective", *J. Am. Ceram. Soc.*, **92** [5] (2009) 967–983.